Astrophys Space Sci (2016) 361:46
DOI 10.1007/s10509-015-2630-y

ORIGINAL ARTICLE

A 3D model for α Gem AB: orbits and dynamics

José A. Docobo[1,2] · Manuel Andrade[1,3] · Pedro P. Campo[1] · Josefina F. Ling[1,2]

Received: 28 July 2015 / Accepted: 13 December 2015

Abstract The well-known multiple star system, Castor, and particularly, the [(Aa, Ab), (Ba, Bb)] subsystem, was studied in detail. After a rigorous analysis of the quality controls, a new solution for the visual orbit yielded new values for the different physical and orbital parameters of the system. In addition, a comprehensive investigation of the orbital configuration of the quadruple system allowed us to provide both accurate individual masses and orbital inclinations of the spectroscopic subcomponents, as well as a new value of its orbital parallax. Finally, by means of a numerical analysis of the long-term dynamics, we obtained the most probable values of the nodal angles of the two spectroscopic subsystems for the first time.

Furthermore, the full characterization of this remarkable system allowed us to discuss some interesting features of its present configuration. In this way, we concluded that the eccentric (Aa, Ab) subsystem is yet undergoing Kozai-Lidov cycles whereas, on the contrary, the circular (Ba, Bb) subsystem has probably already reached a stable stage.

Keywords Astrometry · Celestial mechanics · Binaries: spectroscopic · Binaries: visual · Stars: fundamental parameters · Stars: α Gem AB (Castor)

✉ M. Andrade
manuel.andrade@usc.es

[1] R.M. Aller Astronomical Observatory, University of Santiago de Compostela, Santiago de Compostela 15782, Galiza, Spain

[2] Departamento de Matemática Aplicada, Facultade de Matemáticas, University of Santiago de Compostela, Santiago de Compostela 15782, Galiza, Spain

[3] Departamento de Matemática Aplicada, Escola Politécnica Superior, University of Santiago de Compostela, Lugo 27002, Galiza, Spain

1 Introduction

When W.D. Heintz published his results regarding Castor (α Geminorum) in 1988, he wrote that this system did not really need to be introduced, and he was correct. Castor is probably one of the most studied hierarchical multiple star systems. Consequently, ample scientific literature exists that concerns it.

As is well known, the visual system consists of three stars: A, B, and C, in such a way that A and B constitute a long-period binary with brilliant components, white in colour. Nevertheless, the eclipsing binary, YY Geminorum, is gravitationally associated with the system and is, therefore, the component C. The three stars: A, B, and C are single-lined binaries, for which the system is a sextuplet.

These six components: Aa, Ab, Ba, Bb, Ca, and Cb (see Fig. 1) form a stable dynamic system that is defined by five orbits. Three of them have a very short period that corresponds with the spectroscopic pairs (Aa, Ab) (9.2128 days), (Ba, Bb) (2.9283 days), and (Ca, Cb) (0.8143 days). These orbital elements have been well determined for a long time (Vinter Hansen 1940 for the systems A and B, and Ségransan et al. 2000 for system C). They are included in the *S_{B^9}: The Ninth Catalogue of Spectroscopic Binary Orbits* (Pourbaix et al. 2004).

Lastly, the orbit of the AB pair (actually, (Aa, Ab), (Ba, Bb)) has now moved 300 degrees since Bradley and Pound discovered Castor to be a double star at the beginning of the 18th century having been permanently tracked by means of different observation techniques.

The resolution of the A and B components in X-ray light by the *Chandra X-ray Observatory* has informed us that both are highly variable and are frequently subject to flaring (Stelzer and Burwitz 2003). Due to the similarity of these flares as compared with those in dMe flares stars, it

Published online: 31 December 2015

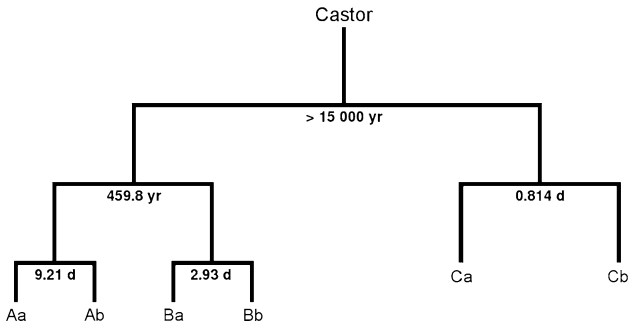

Fig. 1 Mobile diagram of Castor

is commonly accepted that this X-ray emission is caused by the late-type companion in each subsystem (Pallavicini et al. 1990).

Although the eclipsing YY Geminorum subsystem is of special astrophysical interest and, as such, is being studied by numerous scientists, its small mass and its significant distance (as compared with the rest of the system) hardly affects the dynamics of the other components. Moreover, because the elements of the very long period orbit of the distant companion, C, remain unknown, it is not practical to initiate a global study of α Geminorum. For that reason, we have focused on the quadruple system, [(Aa, Ab), (Ba, Bb)], in this report and conducted an exhaustive investigation regarding the dynamics of the same.

Following this Introduction, we present a new orbit of system AB in Sect. 2, having utilised all of the observational material available: visual, photographic, CCD, and speckle measurements. The proposed solution, that has better quality controls as compared to previously calculated orbits, will be that which is used in the rest of this study. We call this orbit, Orbit 2. Orbit 1 will be that of the spectroscopic pair: (Aa, Ab). Orbit 3 corresponds to the other spectroscopic pair: (Ba, Bb). Alternatively, we also give the name "inner pairs" to the orbits 1 and 3 and "outer pair" to orbit 2.

In Sect. 3, using an ad-hoc version of the methodology designed by Docobo and Andrade (2006) for the study of stellar systems with spectroscopic components, we contribute the values of the semimajor axes and inclinations of orbits 1 and 3, as well as the parallax of the system and, consequently, of the masses and spectral types of the four components. In addition, the dynamical analysis carried out in Sect. 4 will allow us to estimate the most probable values of the nodal angles of orbits 1 and 3 as well as indicate some constraints with respect to the long-term evolution of the quadruple system.

2 A new orbit for the AB system

The first orbit of the [(Aa, Ab), (Ba, Bb)] system (henceforth, AB) was calculated by John Herschel in 1832. Since then numerous solutions have been contributed, the latest being those of Muller (1956), Rabe (1958), Walbaum and Duvent (1983), Docobo and Costa (1987), Heintz (1988), De Rosa et al. (2012), Docobo et al. (2014), Matvienko et al. (2015).

Table 1 contains the elements of these orbits. It also includes the grade assigned to each one of them according to the criteria utilized by USNO in *The Sixth Catalog of Orbits of Visual Binary Stars* (Hartkopf et al. 2001) as well as the values of the quality controls (in θ and ρ) in terms of the root mean square (RMS). In light of the results contained in these tables, one may conclude that, except for the orbital period (probably between 450 and 470 years), the rest of the elements are now satisfactorily defined.

With the idea of obtaining an orbit that best fits the set of available observations, we have proceeded to compile all of

Table 1 Orbital elements (with uncertainties, if available) for Castor AB, USNO grades (G), and orbital quality controls in RMS (the best numbers are highlighted in *bold*)

Author(s)	P [yr]	T	e	a [″]	i [°]	Ω [°]	ω [°]	G	RMS	
									θ [°]	ρ [″]
[1] Muller (1956)	511.3	1950.65	0.360	7.369	112.94	41.65	239.81	3.9	1.55	0.156
[2] Rabe (1958)	420.07	1965.3	0.330	6.295	115.94	40.47	261.43	3.8	2.62	0.141
[3] Walbaum and Duvent (1983)	393.46	1970.09	0.33	5.948	116.9	39.58	269.18	3.4	4.02	0.166
[4] Docobo and Costa (1987)	444.95	1960.10	0.323	6.593	114.6	41.5	253.3	3.4	1.10	**0.137**
[5] Heintz (1988)	467.0	1958.0	0.343	6.805	114.5	41.3	249.5	3.4	**0.99**	**0.138**
[6] De Rosa et al. (2012)	$466.8^{+6.3}_{-6.1}$	1957.3 ± 0.3	$0.333^{+0.007}_{-0.006}$	6.78 ± 0.05	113.56 ± 0.09	41.2 ± 0.1	$249.3^{+0.6}_{-0.5}$	3.2	1.32	0.143
[7] Docobo et al. (2014)	459.8	1958.7	0.336	6.755	114.6	41.2	250.5	3.1	**0.99**	**0.138**
[8] Matvienko et al. (2015)	453.6 ± 0.8	1958.1 ± 0.4	0.326 ± 0.002	6.69 ± 0.03	114.2 ± 0.2	40.3 ± 0.2	248.8 ± 0.5	3.2	1.17	0.150
[9] This work	459.8 ± 4.2	1959.1 ± 0.9	0.337 ± 0.004	6.732 ± 0.043	114.7 ± 0.3	41.3 ± 0.2	251.1 ± 1.4	3.1	**0.98**	**0.138**

Table 2 The percentage of weight contributed by the different observations

	Visual	Photographic	CCD	Speckle
Weight [%]	65.4	7.4	11.2	16.0

Table 3 The last observations used in the calculation of the new orbit

t	θ [°]	ρ [″]
2014.3680	55.0	5.02
2014.3980	54.8	5.02
2015.1839	54.7	5.05
2015.1865	54.5	5.06
Observer: J.A. Docobo		
Technique: visual (micrometer)		
Telescope: 0.62 m (OARMA)		

the existing observational material which has been provided to us by the USNO (Hartkopf 2014). In total, we have made use of 1416 observations of which 1120 are visual, 165 are photographic, 55 are CCD images, and 76 are speckle interferometric measurements.

As a function of the number of nights that correspond to each observation, the technique employed, the observer, and the telescope used, each measurement was assigned a weight according to the criteria established by USNO itself (Hartkopf 2014). Table 2 presents the percentage of weight contributed by the measurements obtained with each technique. The last observations used were performed in 2014 and 2015 by one of the authors of this article (J.A.D.), using a micrometer attached to the 0.62 m telescope of the *Ramón María Aller Astronomical Observatory* (OARMA) (see Table 3). All of the observations were corrected by precession for the epoch, J2000.0.

The method used to obtain a new orbit was proposed by Docobo (1985, 2012) with which more than 300 orbits have been calculated in recent decades. As is well known, this method consists of establishing an application: $V \rightarrow (P, T, e, a, i, \Omega, \omega)$ from the interval $(0, 2\pi)$ into the set of elliptical Keplerian orbits whose corresponding apparent orbits pass through three previously fixed points $(\theta_i, \rho_i; t_i)_{i=1,2,3}$. These points must obviously belong to areas with maximum of observation evidence in their favour.

From the set of generated orbits, the selection can be made according to different criteria: a minimum RMS (square root of the mean of the squares of the residuals) and/or a minimum AM (arithmetic mean of the residuals) in θ and ρ, the computed parallax which most closely approximates that measured by *Hipparcos*, deduced masses that correspond to the spectral types, etc. Using this method, it is not necessary to calculate the areal constant as occurs, e.g., in the Thiele-Innes-Van den Bos method.

After analysing the complete collection of the observations, we proceeded to choose several sets of three points and applied the mentioned orbit calculation method. We obtained different orbits with periods between 443 and 468 years that reasonably well fit the observations. A rigorous selection accomplished using the minimum RMS/AM criterion led us to a concrete orbit. Finally, we minimized their residuals using a gradient descent algorithm in order to improve the solution. The orbital elements along with the corresponding standard uncertainties are listed in Table 1.

The new orbit, that is quite similar to another that we calculated last year, will be used in the following sections. In accordance with the USNO criterion, the corresponding grade of this orbit is 3.1 (Hartkopf 2015). In Fig. 2, we present the apparent orbit of the new solution with the visual, photographic, CCD, and speckle measurements, respectively.

3 A quasi-3D model

As mentioned earlier, we are studying a quadruple stellar system which comprises a visual binary wherein both components are spectroscopic binaries. Although visual (outer), as well as spectroscopic (inner) orbits are well known as we have seen in Sects. 1 and 2, many astrometric and astrophysical parameters remain unknown.

Nevertheless, we can overcome this problem by applying a procedure (Docobo and Andrade 2006) which allows us to obtain many astrometric and astrophysical parameters in order to provide a more detailed description of this system. This approach takes advantage of many implicit relations that arise in a three-body stellar system.

In this case, however, we must take into consideration that Castor AB is a hierarchical quadruple stellar system, therefore, we will use a modified version of the aforementioned procedure. The major change will consist of using the *Hipparcos* parallax instead of an intermediate mean parallax for each triple system throughout the procedure.

First, we take the orbital elements of both spectroscopic orbits (P_A, $k_{A,1}$, e_A; P_B, $k_{B,1}$, e_B) from the S_{B^9}, the combined apparent magnitudes of each subcomponent of the visual pair ($m_A \equiv m_{AaAb}$, $m_B \equiv m_{BaBb}$) from the WDS, and the trigonometric parallax from *The Hipparcos Catalogue*. The former allows us to calculate the mass functions and thus to estimate minimum masses and later spectral types of the second components in both spectroscopic subsystems.

The next step is to estimate the most appropriate range for the absolute magnitudes of the spectroscopic subcomponents in each subsystem by using Jaschek's criterion (Jaschek and Jaschek 1987) according to which, in the case of SB1, only stars that differ by less than about 1 magnitude are observable as a composite spectrum. Then, mean values of the absolute magnitudes for each component (M_{Aa}, M_{Ab}, M_{Ba}, M_{Bb}) can be estimated by applying the procedure to

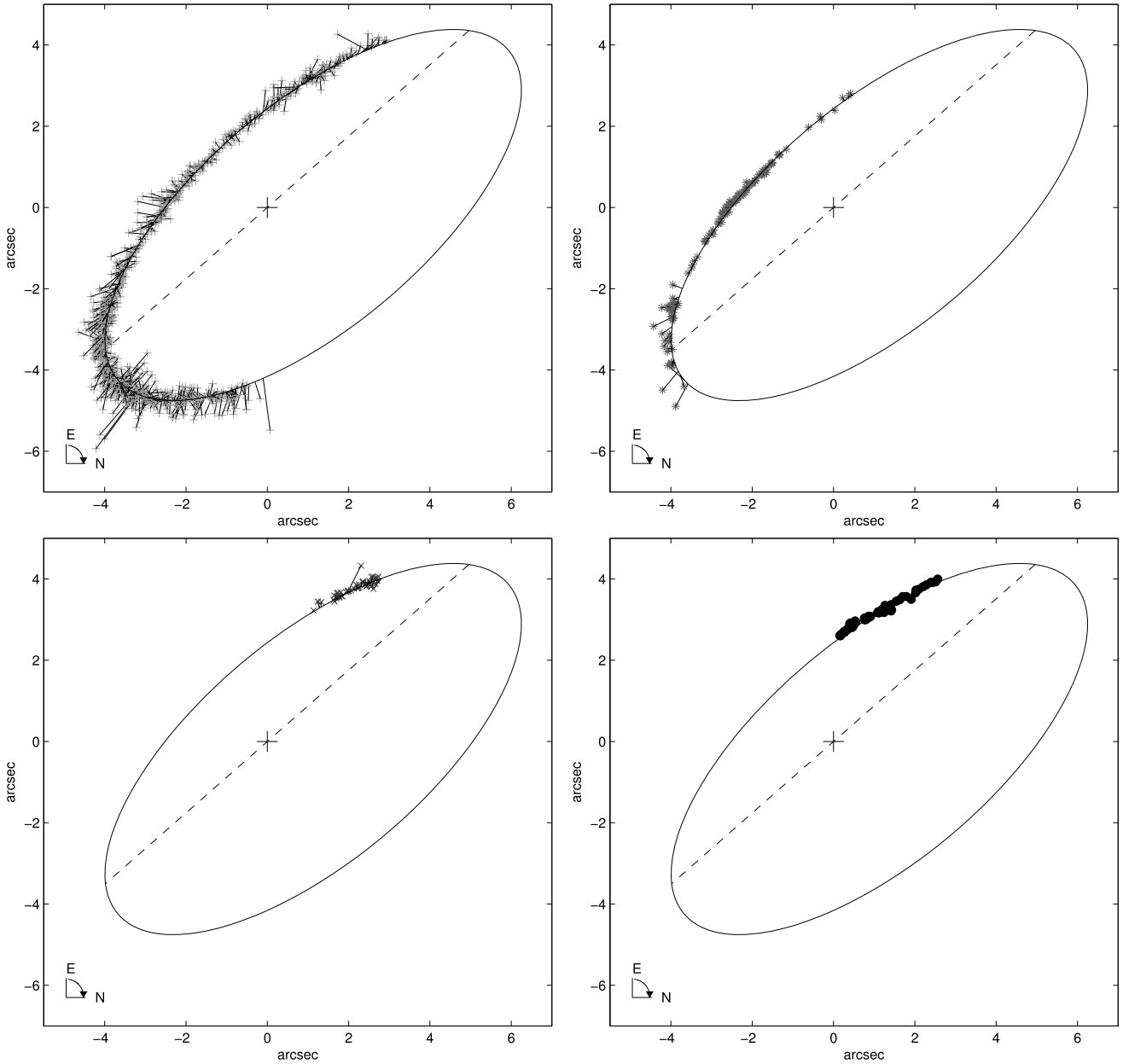

Fig. 2 Apparent orbit with visual (*top left*), photographic (*top right*), CCD (*bottom left*) and speckle (*bottom right*) measurements

each spectroscopic subsystem independently and considering only those values compatible with the *Hipparcos* parallax by means of the expression

$$\log \pi = \frac{M_1 - m_{12} - 5}{5} - \frac{1}{2}\log\left(1 + 10^{-0.4\Delta M}\right), \qquad (1)$$

where π is the parallax corresponding to each value of the absolute magnitude of the first component in the spectroscopic binary, M_1 ($= M_{Aa}$ or M_{Ba}), and to each value of the difference between the magnitudes of both components, $\Delta M = M_2 - M_1$ ($= M_{Ab} - M_{Aa}$ or $M_{Bb} - M_{Ba}$). In addition, m_{12} is the combined visual apparent magnitude of the spectroscopic binary ($= m_A$ or m_B). Then, for the mean values of M_1 and $\pi_{\rm Hip}$, we calculate the corresponding values of M_2 (obtained from ΔM) and M_3 (inferred from m_3, the visual apparent magnitude of the distant companion, and $\pi_{\rm Hip}$).

Moreover, individual masses and spectral types for each component can be calculated using the suitable calibrations (see Sect. 3.1).

At this point, well-determined visual orbital elements of the AB system (namely, period and semimajor axis) are crucial to calculate the orbital parallax as well as the inclinations and the semimajor axes of both spectroscopic orbits

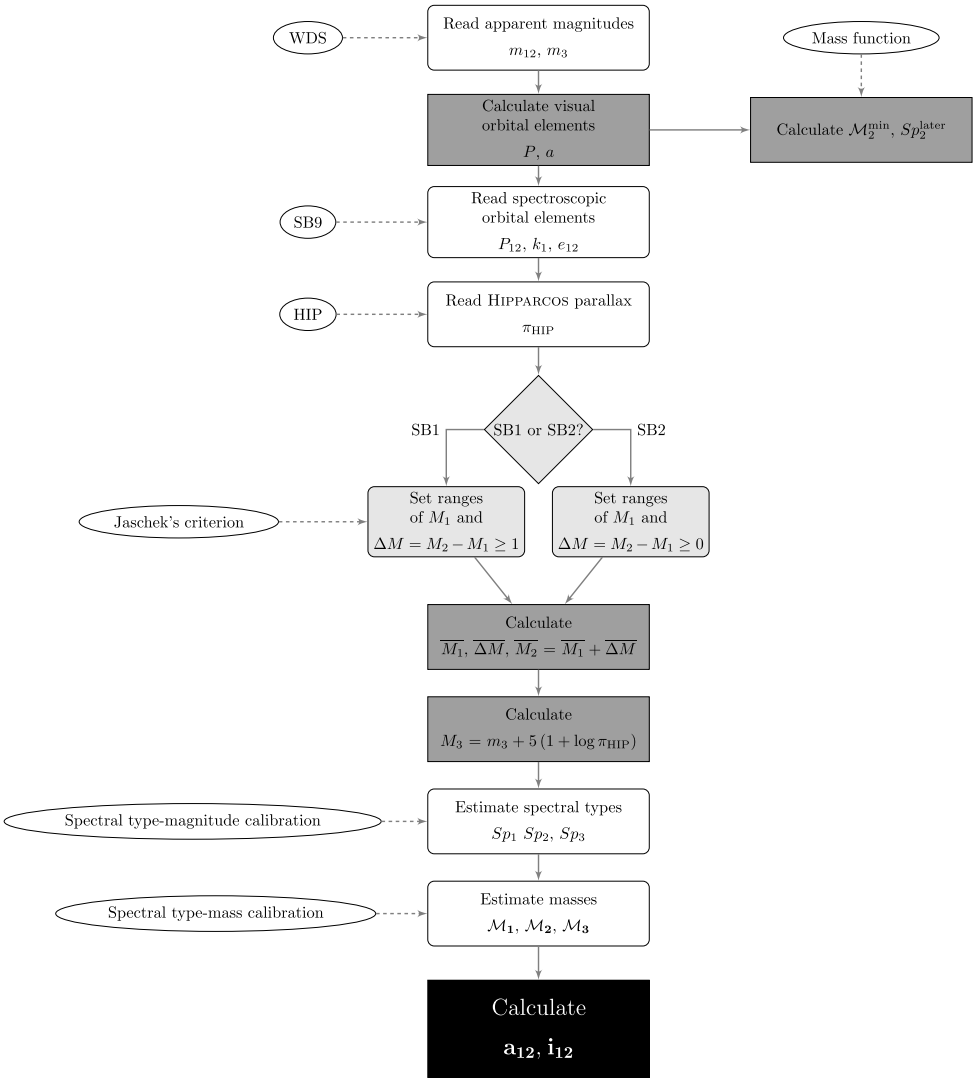

Fig. 3 The flowchart of the Docobo and Andrade (2006) methodology as applied to this particular case

(see Sect. 3.2). A flowchart that describes this methodology is shown in Fig. 3. Furthermore, a detailed description with examples can be seen in Docobo and Andrade (2006).

In the end, the only orbital elements that will remain unknown will be the inner angles of the nodes, Ω_1 and Ω_3, of the spectroscopic subsystems. For that reason, we call this a quasi-3D model. Further on in this paper, we will offer a few clues regarding the estimation of plausible values for these orbital elements.

3.1 Computation of the individual masses and spectral types

This procedure also provides individual masses and spectral types which are listed in Table 4. We conclude that each binary subsystem comprises a massive component of spectral type A along with a cool dwarf companion of spectral type M, the latter accounting for a fifth of the total mass of each subsystem.

Table 4 Spectral types and derived individual masses

	Sp	M [$M_\odot$]
Aa	A2V	2.57 ± 0.11
Ab	M0V	0.53 ± 0.09
Ba	A5V	2.13 ± 0.10
Bb	M1V	0.49 ± 0.09
Total		5.72 ± 0.20

These individual masses are somewhat larger than those obtained in previous studies (Heintz 1988; Torres and Ribas 2002) but this is easy to understand if we take into account that they used larger values of the parallax. In reality, the new total mass obtained in this work from the sum of individual masses (5.72 ± 0.20 $M_\odot$) matches well with the dynamical mass obtained from orbital elements together with the *Hipparcos* parallax, that is, 5.47 ± 0.97 $M_\odot$. Actually, this match is even better if we take into consideration the old *Hipparcos* reduction (5.70 ± 0.36 $M_\odot$).

Table 5 Semimajor axes, inclinations, largest angular separations, and differences of magnitudes of the spectroscopic subsystems

Subsystem	a [au]	a [mas]	i [°]	$\rho_{\max}$ [mas]	Δm
(Aa, Ab)	0.127 ± 0.007	8.17 ± 0.68	25.6 ± 4.3	11.1 ± 1.0	7.6
(Ba, Bb)	0.0562 ± 0.0033	3.61 ± 0.30	53.9 ± 13.0	3.61 ± 0.30	7.5

Indeed, the fractional mass given by

$$f = \frac{M_B}{M_A + M_B}, \tag{2}$$

where M_A and M_B are the masses of the A and B spectroscopic subsystems, respectively, turns out to be 0.458 ± 0.017. That is, it is only slightly larger than that given by Heintz (1988), 0.436 ± 0.003, obtained from relative positions of stars A and B with respect to star C (YY Gem).

3.2 Computation of the semimajor axes and inclinations of the spectroscopic orbits

By using the new visual orbit (this work) in conjunction with the two spectroscopic orbits Vinter Hansen (1940) and the Hipparcos parallax, we have calculated the most probable values of both the separations between their components as well as of the spectroscopic binary inclinations using the above-mentioned Docobo and Andrade (2006) methodology according to the following relationships:

$$a_{12} = a\left[\left(\frac{P_{12}}{P}\right)^2\left(\frac{M_1 + M_2}{M}\right)\right]^{1/3}, \tag{3}$$

$$a_1 \sin i_{12}\ (\text{in km}) = 13751 K_1 P_{12}\left(1 - e_{12}^2\right)^{1/2}, \tag{4}$$

where a_{12}, i_{12}, e_{12}, and P_{12} are the semimajor axis, the inclination, the eccentricity and the period of each spectroscopic subsystem, respectively. On the other hand, M, M_1, and M_2 are the total mass and the masses of each component, respectively. In addition, $a_1 = a_{12}\frac{M_2}{M_1+M_2}$.

Furthermore, regarding an eventual observation of the spectroscopic subcomponents by means of optical techniques, we have also estimated their largest angular separations. Table 5 summarizes these results along with the differences of magnitudes between the components according to the Straižys and Kuriliene (1981) calibration.

These semimajor axes well match those estimated by M. Güdel, 0.121 and 0.052 au, respectively, in a private communication quoted by Stelzer and Burwitz (2003). Likewise, the inclinations are in reasonable agreement with those roughly estimated by Torres and Ribas (2002) for the (Aa, Ab) and (Ba, Bb) subsystems, ($\sim 28°$) and ($\sim 90°$), respectively.

3.3 Computation of the parallax

Regarding the system parallax, we have computed the orbital parallax (derived from the new visual orbit, AB, along with the new estimation of the total mass). This is listed in Table 6 together with the trigonometric parallaxes measured by the *Hipparcos* mission (old and new reductions) and with those given by Heintz (1988) and Torres and Ribas (2002).

Table 6 Comparison of parallaxes

	Parallax [mas]
Trigonometric (I) (Heintz 1988)	73
Trigonometric (II) (Heintz 1988)	65.5
Trigonometric (ESA 1997)	63.27 ± 1.23
Trigonometric[a] (Torres and Ribas 2002)	66.90 ± 0.63
Trigonometric (van Leeuwen 2007)	64.12 ± 3.75
Orbital (this work)	63.19 ± 0.92

[a]This was re-reduced from the *Hipparcos* transit data (ESA 1997) accounting for the orbital motion of the visual binary

We note that the old *Hipparcos* trigonometric parallax is slightly smaller than the new one but, in comparison, the former almost exactly matches the accurate orbital parallax calculated in this work. This type of discrepancy between the parallaxes given by the old and the new reductions of the *Hipparcos* data when the old value seems to be more accurate, has occurred previously (Docobo and Andrade 2013).

4 Dynamical analysis and the 3D model

4.1 Aims and models

Considering that we have no initial knowledge of the angles of the nodes of the spectroscopic subsystems in addition to the fact that the ratios between the orbital period of the outer orbit and each of the smallest orbital periods of the inner orbits are huge (roughly $6 \cdot 10^4$), the implementation of many direct integrations of the motion equations of this four-body problem is not practical. From another standpoint, such huge ratios have led some authors (Anosova et al. 1989; Beust 2003) to conclude that the nearly circular binary (Ba, Bb) is very stable. In fact, as suggested by Schmitt et al. (1994), it would be in synchronous rotation.

Taking all of this into account, in order to accomplish an analysis of the long-term dynamics of α Gem AB, we will consider that each binary subsystem operates as a one-body perturber on the other binary subsystem. Thus, we will focus our attention on the following systems:

1. [(Aa, Ab), B] and
2. [(Ba, Bb), A].

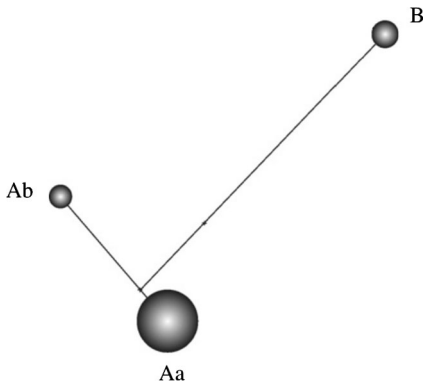

Fig. 4 System of Jacobi coordinates for a three-body system (distances and sizes are not to scale)

During this investigation, we hope to eventually be able to determine those regions of the orbital elements space with the most probable values for the inner angles of the nodes.

Assuming the above-mentioned facts, our model will be that of a hierarchical three-body system characterized by an Ab body in an elliptical inner orbit around the Aa body and a third body, B, moving in an outer elliptical orbit around the centre of mass of the subsystem (Aa, Ab) as shown in Fig. 4 (and similarly in case (ii)). As usual, we will work with the system of Jacobi coordinates.

According to the Mardling and Aarseth (2001) stability criterion valid for non-coplanar systems, one body may escape from a hierarchical three-body system if it obeys:

$$\frac{r_p^{\rm out}}{a_{\rm in}} < 2.8\left[(1+q_{\rm out})\frac{1+e_{\rm out}}{(1-e_{\rm out})^{1/2}}\right]^{2/5}\left(1-\frac{0.3I[^\circ]}{180}\right), \quad (5)$$

where $e_{\rm out}$ and $r_p^{\rm out}$ are the outer eccentricity and periastron separation, $q_{\rm in} = M_2/M_1$ and $q_{\rm out} = M_3/(M_1+M_2)$ are the inner and outer mass ratios, respectively, $a_{\rm in}$ is the inner semimajor axis, and $I[^\circ]$ is the mutual inclination in degrees.

Regarding the stability of the α Gem [(Aa, Ab), B] and [(Ba, Bb), A] systems, this criterion is not satisfied by a very wide margin independent of the value considered for the inner angles of the nodes. Other modern criteria such as that of Valtonen and Karttunen (2006) yield very similar results.

A summary of the entire set of orbital data concerning this stellar system used in the calculations is presented in Table 7.

With the aim of distinguishing the main dynamical features of these three-body systems and, afterwards, to determine the most probable values of the nodes, we will study some aspects of their secular dynamics.

4.2 Constraints in the inner angles of the nodes

First, we will ascertain the set of allowed mutual inclinations determined by the remaining orbital elements using the well-known expression:

$$\cos I = \cos i_{\rm in}\cos i_{\rm out} + \sin i_{\rm in}\sin i_{\rm out}\cos(\Omega_{\rm out}-\Omega_{\rm in}), \quad (6)$$

with I being the mutual inclination between both the inner and outer orbital planes.

Plots displaying the dependencies of the mutual inclination on the inner angle of the node for each subsystem are shown in Fig. 5. These plots allow us to know what combinations of inclinations and angles of the nodes can give rise to the well-known Kozai-Lidov cycles (hereafter, KL cycles) (Kozai 1962; Lidov 1962), a mechanism that transfers angular momentum between the inner and the outer orbits which can happen only if the mutual inclination is large enough (between 39°.2 and 140°.8).

By means of a numerical analysis of Eq. (6), we learn that the [(Aa, Ab), B] system can undergo KL cycles for whichever value of its angle of the node. In contrast to that, the [(Ba, Bb), A] system may or may not undergo KL cycles depending on its angle of the node. Results are shown in Table 8.

When KL cycles are present, long-period oscillations of the inner eccentricity and inclinations are observed. The time scale of these KL cycles, $t_{\rm KL}$, can be estimated (see

Table 7 Summary of the orbital parameters of α Gem AB

	Subsystem 1 (Aa, Ab)[a]	Subsystem 2 (A, B)	Subsystem 3 (Ba, Bb)[a]
P [yr]	$2.52224 \cdot 10^{-2}$	459.8 ± 4.2	$8.017180 \cdot 10^{-3}$
T	1934.288668 ± 0.000077	1959.1 ± 0.9	1934.173037 ± 0.000309
e	0.499 ± 0.010	0.337 ± 0.004	0.002 ± 0.004
a [au]	0.127 ± 0.007	105.0 ± 6.2	0.0562 ± 0.0033
i [°]	25.6 ± 4.3	114.7 ± 0.3	53.9 ± 13.0
Ω [°]	(see Table 10)	41.3 ± 0.2	(see Table 10)
ω [°]	266.4 ± 1.8	251.1 ± 1.4	94.7 ± 13.9

[a] P, T, e, and ω (Vinter Hansen 1940); a, i, Ω, M_1, and M_2 (this work)

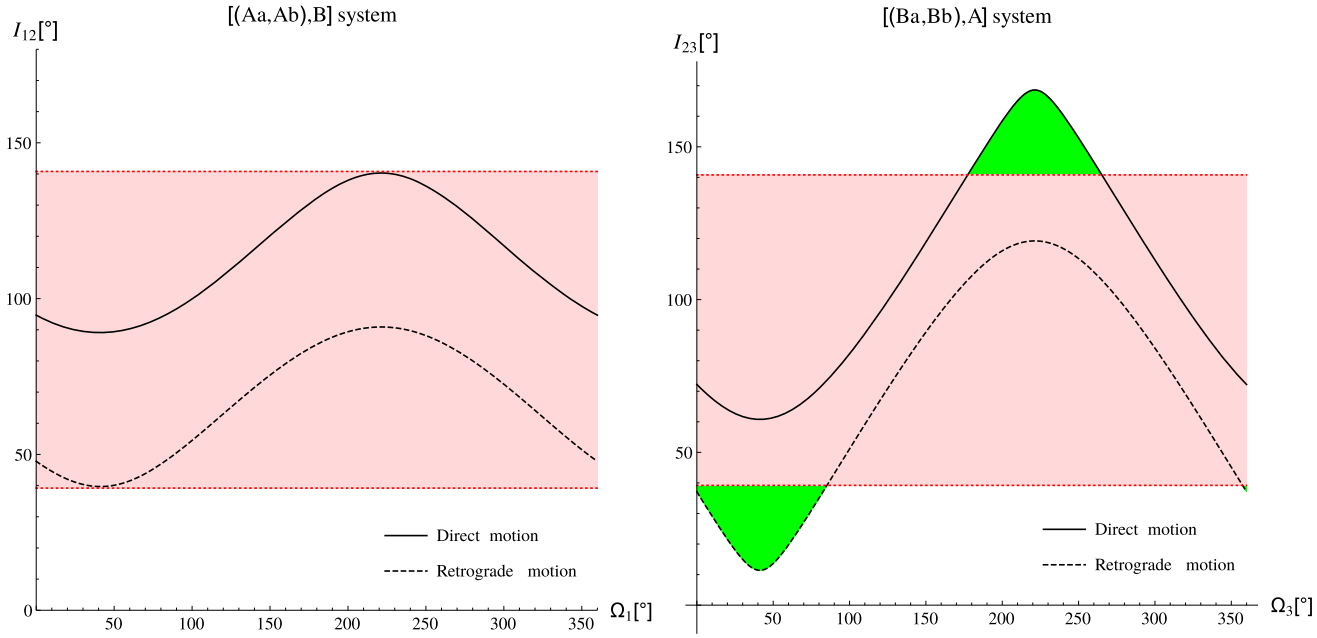

Fig. 5 Plots of the mutual inclinations against the angles of the nodes. The regions where Kozai-Lidov cycles can eventually occur are those shown in *light red*. In contrast, regions where Kozai-Lidov cycles cannot occur are shown in *green*

Table 8 Angles of the nodes, $\Omega_{\rm KL}$, which lead to Kozai-Lidov cycles along with their time scales, $t_{\rm KL}$

Subsystem	$\Omega_{\rm KL}$ [°]	$t_{\rm KL}$ [yr]
(Aa, Ab)	(0.°0, 360.°0)	10^6
(Ba, Bb)	(85.°2, 177.°4) ∪ (265.°2, 357.°4)	10^7

Table 8) using (Li et al. 2014):

$$t_{\rm KL} \simeq \frac{M_{\rm in}}{M_{\rm out}} \left(\frac{a_{\rm out}}{a_{\rm in}}\right)^3 \left(1-e_{\rm out}^2\right)^{3/2} \left(1-e_{\rm in}^2\right)^{1/2} P_{\rm in}, \tag{7}$$

with $M_{\rm in}$ and $M_{\rm out}$ being the mass of the inner binary and the mass of the outer perturber, respectively. The *in* and *out* subindices indicate *inner* and *outer* orbits, respectively.

Therefore, almost circular although highly inclined orbits can become very eccentric over time. In accordance with the assumption that the initial inner eccentricity is small (nearly zero), the quadrupole order expansion of the hierarchical three-body Hamiltonian allows us to calculate the maximum eccentricity, $e_{\rm max}$, that can be induced by the KL cycles depending on the mutual inclination:

$$e_{\rm max} = \sqrt{1-\frac{5}{3}\cos^2 I}. \tag{8}$$

On the other hand, since the mutual inclination can only vary depending on the inner angle of the node, we can solve Eq. (8) in order to know the maximum eccentricities allowed for the angles of the nodes. These curves are shown in Fig. 6.

Additionally, we must take into account that such maximum eccentricities are limited due to the fact that the distance in the periastron should, in any case, be less than the Roche limit. Otherwise, the motion could end in the merging of the system. Thus, in practice, considering the small separations between companions in both subsystems of α Gem AB, the actual maximum eccentricities must be less than those obtained from Eq. (8). In the computation of these upper limits, $e_{\rm max}^{\rm upp}$, we have estimated the effective radii of the Roche lobes, R_L, using the well-known expression (Eggleton 1983):

$$R_L = \frac{0.49q^{2/3}}{0.6q^{2/3}+\ln(1+q^{1/3})}a, \tag{9}$$

where $q = M_1/M_2$. Therefore, we establish the merging condition that the periastron distance must be larger than the Roche limit and, subsequently, that

$$e_{\rm max}^{\rm upp} < 1-\frac{R_L}{a}. \tag{10}$$

In addition, we must also investigate if each system has a lower boundary, $e_{\rm max}^{\rm low}$, determining the existence of minimums in the curves shown in Fig. 6. The results are listed in Table 9.

Again, solving Eq. (8) in an implicit manner, and taking into account the above-mentioned constraints, we obtain the angles of the nodes allowed.

Regarding motion in the (Aa, Ab) subsystem, it undergoes KL cycles for whichever value of its angle of the node.

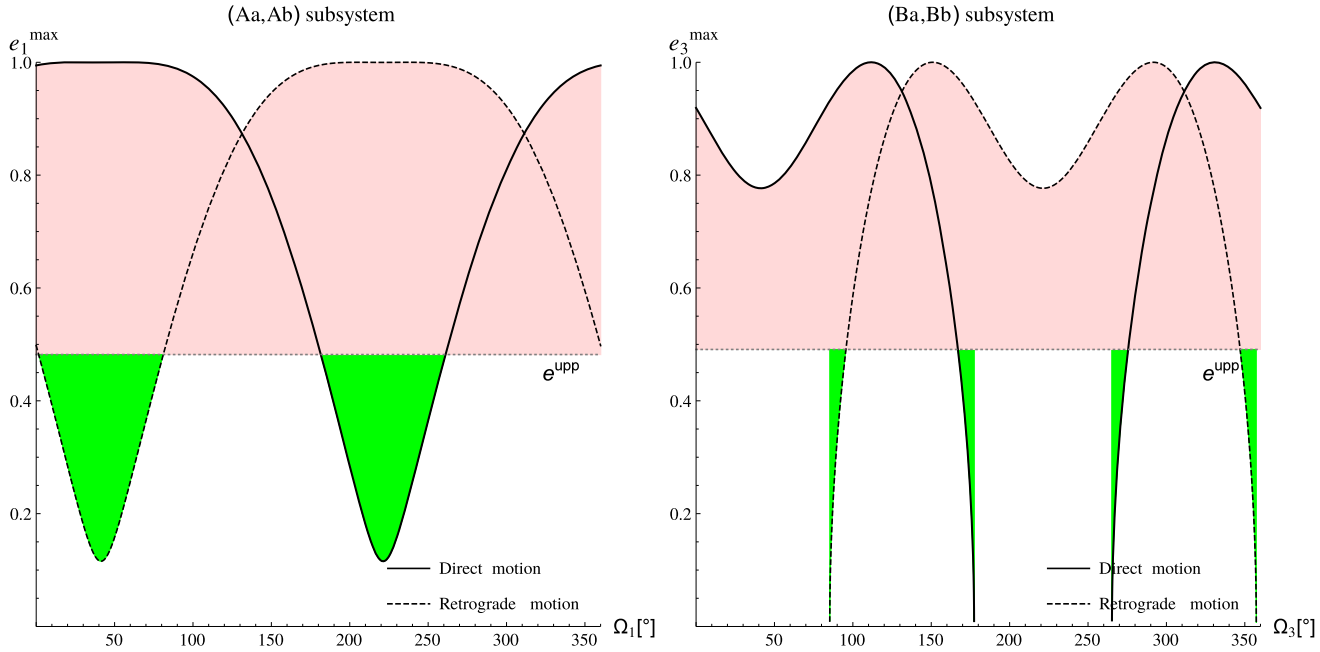

Fig. 6 Plots of the maximum eccentricities, due to the Kozai-Lidov cycles, against the angles of the nodes. Regions where the maximum eccentricity is less than $e_{\max}^{\text{upp}}$ and, therefore, motion is allowed, are shown in *green*. In contrast, those where motion is not allowed are shown in *light red*

Table 9 Stellar radii (R), distances in the periastra (r_p), Roche limits (R_L), and boundaries for the maximum eccentricities due to the Kozai-Lidov cycles ($e_{\max}^{\text{low}}$) and to the merging condition ($e_{\max}^{\text{upp}}$)

Subsystem	$R_a + R_b$ [$R_\odot$][a]	r_p [$R_\odot$]	R_L [$R_\odot$]	$e_{\max}^{\text{low}}$	$e_{\max}^{\text{upp}}$
(Aa, Ab)	$2.0 + 0.60$	13.8 ± 0.8	14.2 ± 0.4	0.116	0.482 ± 0.015
(Ba, Bb)	$1.7 + 0.54$	12.1 ± 0.7	6.1 ± 0.2	0.000	0.491 ± 0.016

[a]Estimated using the Straižys and Kuriliene (1981) calibration from masses

This should be roughly between 178.°9 and 263.°7 (direct motion) or 358.°9 and 83.°7 (retrograde motion). In fact, any other value would lead to extreme KL cycles that could eventually result in the merging of both components.

In regard to the (Ba, Bb) subsystem, we must distinguish two cases: if it is undergoing KL cycles, its angle of the node would vary from 167.°0 to 177.°3, and from 265.°3 to 275.°6 (direct motion) or from 85.°3 to 95.°6, and from 347.°0 to 357.°3 (retrograde motion). Otherwise, it could vary from 177.°3 to 265.°3 (direct motion), and from 357.°3 to 85.°3 (retrograde motion).

The windows of feasible values of the angles of the nodes obtained from a dynamical analysis can be used to determine the expected values for such orbital elements.

4.2.1 Expected angle of the node for (Aa, Ab)

Taking into account the aforementioned merging condition, the allowed interval for the maximum eccentricity caused by KL cycles is also constrained by the current value of the eccentricity. In fact, the latter cannot be larger than its upper boundary for a given KL cycle. As a consequence, in this case, the $e_{\max}$ corresponding to the present configuration must be confined to the interval ($e_{\max}^{\text{low}}$, $e_{\max}^{\text{upp}}$), that is, (0.116, 0.482).

In this respect, the actual eccentricity closely matches its upper boundary. This suggests that this binary would be in the maximum eccentricity stage corresponding to the present KL cycle. In this way, four possibilities around each extreme value arise for the angle of the node: two in direct motion and another two in retrograde motion (see Table 10).

4.2.2 Expected angle of the node for (Ba, Bb)

Under the same assumptions, $e_{\max}$ must be confined to the interval (0.000, 0.491). Taking into account that the current eccentricity is practically zero as well as that this binary is likely undergoing tidal locking (Schmitt et al. 1994), we suggest that the KL mechanism is no longer driving this system. Thus, we propose the means corresponding to each re-

Table 10 The most probable angles of the nodes

Subsystem	Direct motion	Retrograde motion
(Aa, Ab)	$180\overset{\circ}{.}2 \pm 1\overset{\circ}{.}9$	$0\overset{\circ}{.}2 \pm 1\overset{\circ}{.}9$
	$262\overset{\circ}{.}4 \pm 1\overset{\circ}{.}9$	$82\overset{\circ}{.}4 \pm 2\overset{\circ}{.}1$
(Ba, Bb)	$221\overset{\circ}{.}3 \pm 31\overset{\circ}{.}0$	$41\overset{\circ}{.}3 \pm 31\overset{\circ}{.}0$

Table 11 Combinations of allowed mutual inclinations

System	Direct motion	Retrograde motion
[(Aa, Ab), B]	$132\overset{\circ}{.}3 \pm 2\overset{\circ}{.}6$	$47\overset{\circ}{.}7 \pm 3\overset{\circ}{.}5$
[(Ba, Bb), A]	$168\overset{\circ}{.}6 \pm 13\overset{\circ}{.}0$	$11\overset{\circ}{.}4 \pm 13\overset{\circ}{.}0$

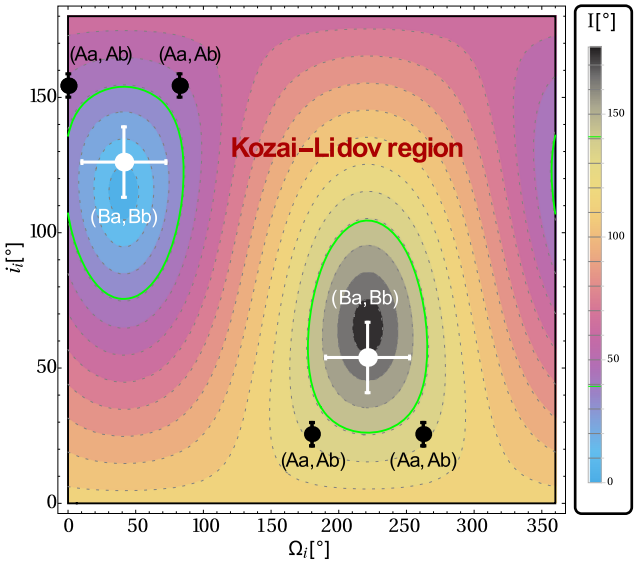

Fig. 7 Contour plot of the mutual inclinations depending on the angle of the node and the inclination of each inner orbit. Positions related to the (Aa, Ab) and (Ba, Bb) subsystems are coloured in *black* and *white*, respectively. *Bars* show standard uncertainties. Regions that are free of Kozai-Lidov cycles are those inside the *green lines*. The *upper* one corresponds to binaries with direct motion, whereas the *lower* one is where the binaries exhibit retrograde motion

gion free of KL cycles as the most probable values for the angle of the node. As a consequence, uncertainties are larger than in the (Aa, Ab) case. Results are also listed in Table 10.

4.3 Long-term mutual inclinations

Taking into consideration the complete set of combinations among these angles of the nodes as well as Eq. (6), we can calculate what mutual inclinations are allowed for the entire system. Those are summarized in Table 11 and their values along with the corresponding angles of the nodes are shown using a contour plot in Fig. 7.

In agreement with the analysis carried out earlier, we can assert that the [(Aa, Ab), B] system would be undergoing KL cycles whether the motion is direct or not. On the contrary, the [(Ba, Bb), A] system would have passed this phase and, in any case, its mutual inclination would be relatively low at present.

Regarding more bizarre features such as an eventual flip of the orbital plane of any of these systems, we have tested the analytical criterion given by Li et al. (2014). According to that, an eccentric inner orbit with an initial near-coplanar configuration in a hierarchical three-body system with an eccentric outer perturber can flip its orientation by about 180° if the parameter, ϵ, measuring the relative significance of the octupole to quadrupole term (Naoz et al. 2013),

$$\epsilon = \frac{M_a - M_b}{M_a + M_b} \frac{a_{\rm in}}{a_{\rm out}} \frac{e_{\rm out}}{1 - e_{\rm out}^2}, \tag{11}$$

where M_a and M_b are the masses of the inner companions and *in* and *out* subindices indicate *inner* and *outer* orbits, respectively, is larger than ϵ_c,

$$\epsilon_c = \frac{8}{5} \frac{1 - e_{\rm in}^2}{7 - e_{\rm in}(4 + 3e_{\rm in}^2)\cos(\omega_{\rm in} + \Omega_{\rm in})}. \tag{12}$$

The ϵ/ϵ_c ratios of the both [(Aa, Ab), B] and [(Ba, Bb), A] systems are on the order of 10^{-3} and 10^{-4}, respectively. Thus, we should not expect such behaviour in the future evolution of α Gem AB.

4.4 Full orbits for the (Aa, Ab) and (Ba, Bb) subsystems

Due to the above-mentioned constraints concerning the motion of the (Aa, Ab) and (Ba, Bb) binaries, we can complement their sets of orbital elements (see Table 7) with reliable values of the angles of the nodes (see Table 10). Nevertheless, ambiguity concerning the relative direction of motion cannot be eliminated. The apparent orbits are shown in Fig. 8. Note that both directions (direct and retrograde) are possible.

5 Conclusions

1. After an investigation of the most recently calculated orbits for the system, Castor AB, we proceeded to make use of the complete set of observations in order to determine a new solution that generally improves the quality controls of previous orbits, keeping in mind the assigned weights of each observation according to USNO criteria.
2. Using the application of a new ad hoc version of the methodology developed by Docobo and Andrade (2006), we present a quasi-three dimensional model of the four-star system [(Aa, Ab), (Ba, Bb)] at the same time that we offer the most probable values of the masses, spectral types, and magnitudes for each component as well as the parallax.

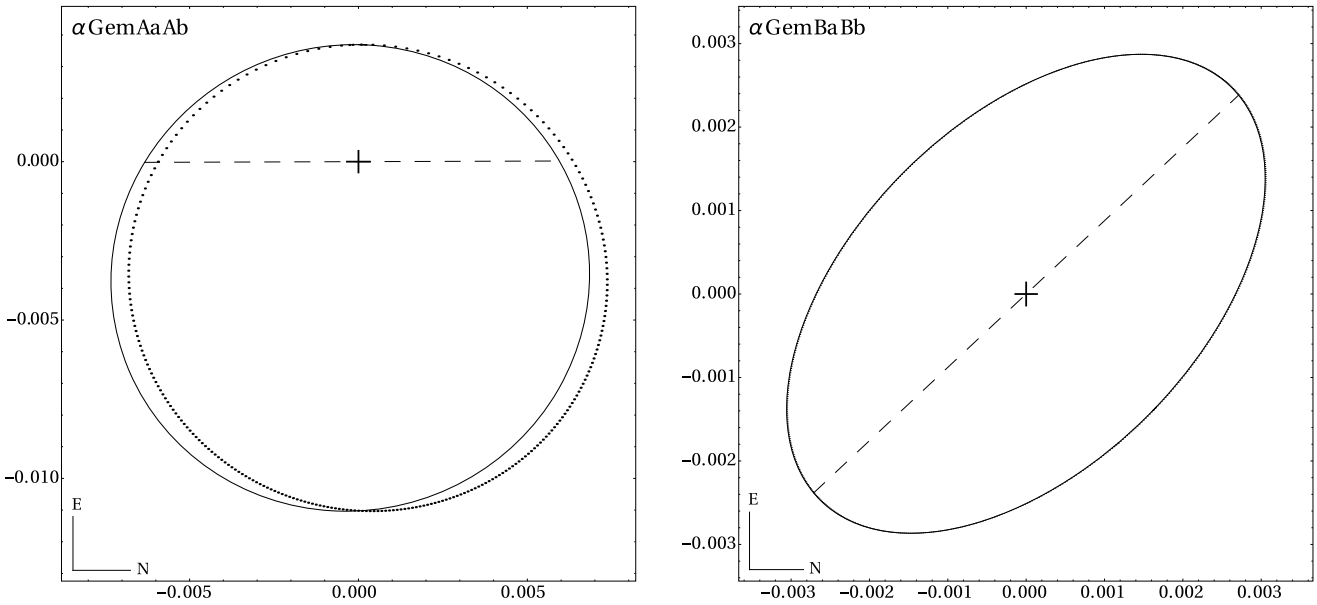

Fig. 8 Apparent orbits for α Gem AaAb (*left*) and α Gem BaBb (*right*). The scale on both axes is in arc seconds and the *dashed line* is the line of nodes. Retrograde motion in the α Gem AaAb orbit is shown using a *dotted line*

3. An exhaustive analysis of the dynamics of the system also permitted us to be able to evaluate the most probable values of the angles of the node for the orbits of the spectroscopic subcomponents (Aa, Ab and Ba, Bb) and, at the same time, to estimate their maximum angular separations as concerns possible optical resolution.
4. Close binaries (with orbital periods of a few days) tend to be circular because of tidal interactions that efficiently circularise initially close eccentric binaries. Taking this into account, we suggest that the (Ba, Bb) subsystem, probably after a phase of high eccentricities caused by KL cycles, has already reached this stage. Therefore, this system would be in a stable circular orbit resistant to the minor perturbations caused by the distant (Aa, Ab) subsystem.
5. On the contrary, the (Aa, Ab) subsystem is still subject to KL cycles that, until now, have avoided an effective circularisation of its orbit. Moreover, its current eccentricity has led this binary to practically cross its Roche limit during the periastron passages. Although we cannot discard that tidal effects as well as general relativity precession could finally suppress KL cycles in a shorter time scale, the dynamical evolution of this binary could end in the merging of both companions.

Acknowledgements The authors thank W. Hartkopf of USNO for providing the data and other relevant information necessary for this research.

This paper was supported by the Spanish *Ministerio de Economía y Competitividad* under Project AYA 2011-26469 as well as by the IEMath-Galicia Network (FEDER-Xunta of Galicia).

References

Anosova, Z.P., Orlov, V.V., Chernyshev, M.V.: Sov. Astron. Lett. **15**, 237 (1989)
Beust, H.: Astron. Astrophys. **400**, 1129 (2003)
De Rosa, R.J., et al.: Mon. Not. R. Astron. Soc. **422**, 2765 (2012)
Docobo, J.A.: Celest. Mech. **36**, 143 (1985)
Docobo, J.A.: In: Arenou, F., Hestroffer, D. (eds.) Proceedings of the Workshop "Orbital Couples: Pas de Deux in the Solar System and the Milky Way", p. 119. Observatoire de Paris, Paris (2012)
Docobo, J.A., Andrade, M.: Astrophys. J. **652**, 681 (2006)
Docobo, J.A., Andrade, M.: Mon. Not. R. Astron. Soc. **428**, 321 (2013)
Docobo, J.A., Costa, J.M.: Pub. Univ. Zaragoza 65–79 (1987)
Docobo, J.A., Andrade, M., Campo, P.P., Ling, J.F.: IAUDS **184**, 1 (2014)
Eggleton, P.P.: Astrophys. J. **268**, 368 (1983)
ESA: The Hipparcos and Tycho Catalogues, ESA SP-1200 (1997)
Hartkopf, W.I.: Private communication (2014)
Hartkopf, W.I.: Private communication (2015)
Hartkopf, W.I., Mason, B.D., Worley, C.E.: Astron. J. **122**, 3472 (2001)
Heintz, W.D.: Publ. Astron. Soc. Pac. **100**, 834 (1988)
Jaschek, C., Jaschek, M.: The Classification of Stars. Cambridge University Press, Cambridge (1987)
Kozai, Y.: Astron. J. **67**, 591 (1962)
Li, G., Naoz, S., Kocsis, B., Loeb, A.: Astrophys. J. **785**, 116 (2014)
Lidov, M.L.: Planet. Space Sci. **9**, 719 (1962)
Mardling, R.A., Aarseth, S.J.: Mon. Not. R. Astron. Soc. **321**, 398 (2001)
Matvienko, A.S., Kiyaeva, O.V., Orlov, V.V.: Astrophys. Lett. **41**, 43 (2015)
Muller, P.: Bull. Astron. Soc. Paris **20**, 145 (1956)
Naoz, S., Farr, W.M., Lithwick, Y., Rasio, F.A., Teyssandier, J.: Mon. Not. R. Astron. Soc. **431**, 2155 (2013)
Pallavicini, R., Tagliaferri, G., Pollock, A.M.T., Schmitt, J.H.M.M., Rosso, C.: Astron. Astrophys. **227**, 483 (1990)
Pourbaix, D., et al.: Astron. Astrophys. **424**, 727 (2004). Available from: http://sb9.astro.ulb.ac.be

Rabe, W.: Astron. Nachr. **284**, 101 (1958)
Schmitt, J.H.M.M., Güdel, M., Predhel, P.: Astron. Astrophys. **287**, 843 (1994)
Ségransan, D., Delfosse, X., Forveille, T., Beuzit, J.-L., Udry, S., Perrier, C., Mayor, M.: Astron. Astrophys. **364**, 665 (2000)
Stelzer, B., Burwitz, V.: Astron. Astrophys. **402**, 719 (2003)
Straižys, V., Kuriliene, G.: Astrophys. Space Sci. **80**, 353 (1981)
Torres, G., Ribas, I.: Astrophys. J. **567**, 1140 (2002)
Valtonen, M., Karttunen, H.: The Three-Body Problem. Cambridge University Press, Cambridge (2006)
van Leeuwen, F.: Astron. Astrophys. **474**, 653 (2007)
Vinter Hansen, J.M.: Publ. Astron. Soc. Pac. **52**, 329 (1940)
Walbaum, M., Duvent, J.-L.: L'Astronomie **97**, 277 (1983)